DOI: 10.13009/EUCASS2025-191
11TH EUROPEAN CONFERENCE FOR AERONAUTICS AND SPACE SCIENCES (EUCASS)

Evaluation of a Variable Cycle Engine for an Engine-Integrated Thermal Management in Fighter Aircraft

Tomasz Matuschek†, Sebastian Zenkner*, Maximilian Weiermann* and Jannik Häßy**
** Institute of Propulsion Technology, German Aerospace Center (DLR)*
Linder Höhe, 51147 Cologne, Germany
tomasz.matuschek@dlr.de – sebastian.zenkner@dlr.de – maximilian.weiermann@dlr.de – jannik.haessy@dlr.de
† Corresponding Author

Abstract

Modern fighter aircraft impose thermal loads that challenge conventional cooling concepts. This study evaluates a closed-air thermal management system (TMS) integrated in two engine architectures: a conventional mixed-flow turbofan and a variable cycle engine (VCE). Across sixteen representative operating points, the VCE consistently meets cooling requirements in most segments and achieves twice the capacity of the conventional engine under supercruise conditions. A temperature – mass-flow study for bypass the conditions reveals that, once bypass flow significantly exceeds the TMS stream, additional cooling is obtained almost exclusively by reducing bypass temperature. Optimizing the VCE variabilities further enlarges the cooling margin at negligible fuel burn penalty, underscoring the thermal and operational advantages as well as the flexibility of variable cycle architectures.

1. Introduction

Thermal loads in modern fighter aircraft applications are growing quickly. Over the past decade the electrical power demand of radars, sensors and mission computers has multiplied, already causing heat loads of several hundred kilowatts up to the low-megawatt range [1,2,3]. The shift toward more-electric architectures and more capable electronic-warfare suites will continue this trend. Planned directed-energy weapons (high-energy lasers, microwaves) intensify the challenge further, because only 25 % of their input power is converted into useful effect while the rest must be removed as heat [2,3].
Traditional cooling devices such as ram-air ducts, compressor bleed air and fuel heat sinks, are now close to their practical limits [3]. Ram-air systems add drag and radar signature; bleed air lowers thrust and efficiency; fuel can absorb heat only while enough mass and temperature margin remain [2,3,4].
These limitations have led to engine-integrated thermal-management concepts. Demonstrators from programs such as AFRL INVENT show the basic feasibility [5]. Variable Cycle Engines (VCE), able to redistribute mass flow between several bypass streams, promise both higher propulsive efficiency and an adjustable heat-sink capacity [6,7,8]. One promising option is to embed a closed air-cycle – a reverse Brayton loop with its own compressor, turbine and heat exchangers – inside the engine and transfer the heat into the bypass flow [2].
The present study investigates how cooling capacity depends on bypass conditions by comparing a conventional mixed turbofan with a core-driven fan engine (CDFE) for a given fighter configuration. After a short literature review, the paper introduces the aircraft and engine models, outlines the integrated TMS, presents the simulation results and closes with the main conclusions.

2. State of the art

Aircraft thermal management includes a wide range of solutions, from simple ram-air channels and fuel heat sinks to multi-stage refrigeration cycles. The review by van Heerden et al. [3] provides a structured overview of architectures and future challenges, highlighting that military platforms require integrated, multifunctional systems because of tight signature, weight and power constraints.
The F-35 Lightning II illustrates the problem. Its Power & Thermal Management System (PTMS) combines an APU with an integrated cooling cycle and supports several operating modes [9]. While the original design could dissipate roughly 30 kW continuously, subsequent capability upgrades are expected to raise the requirement to roughly 80 kW

Copyright © 2025 by First Author. Posted online by the EUCASS association with permission.

DOI: 10.13009/EUCASS2025-191

[10,11]. However, providing this capability requires extra bleed air from the F135 engine, pushing the propulsion system beyond its original design limits and reducing range and life margins [9]. Industry is therefore testing both drop-in PTMS upgrades [12] and improved cooling methods or novel propulsion systems like the application of VCE [6,13]. These developments underline the necessity of defining thermal requirements early in the design process and tightly integrating cooling capabilities into the overall propulsion system [6,7].
One promising approach is to make the engine itself part of the cooling architecture, particularly with Variable-Cycle Engines. Corbett [14] showed that a three-stream VCE can supply several megawatts of shaft power for short periods and discharge the associated heat into a cool outer stream. Clark [6,7] later built an integrated design method for VCE including TMS and demonstrated that adaptive bypass streams allow mission-tailored heat sinks, though his work used an open, bleed-air cycle. Zenkner et al. [8] provide a comprehensive overview of VCE architectures, emphasizing the increased design flexibility they offer – not only for propulsion efficiency and installation benefits, but also for secondary objectives such as thermal management across varying operating conditions.
To date, most published studies have focused on open air cycles or isolated power extraction. A quantitative assessment of a closed air-cycle TMS combined with a variable bypass engine is still lacking. In a previous study [15], the authors of this paper analyzed such a closed-air TMS in a conventional turbofan, identifying limitations due to high bypass temperatures and inherent trade-offs between cooling capacity and engine performance. The current work extends that analysis to a VCE, aiming to quantify how a cooler, continuously flowing outer bypass can enhance the cooling capabilities in a given fighter configuration for defined mission profiles.

3. Application case

This chapter introduces the application case that is used to evaluate an engine-integrated TMS and to compare the two given propulsion architectures. The analysis is based on the virtual fighter-aircraft DLR-FFD (Future Fighter Demonstrator) in combination with the DLR-FFE (Future Fighter Engine). While previous investigations focused on a conventional mixed-flow turbofan [15], the present study additionally considers a variable cycle configuration in the form of a core-driven fan engine (CDFE). The objective is to assess how different engine configurations affect the cooling performance of the TMS for different phases of defined flight missions.

3.1 Future Fighter Demonstrator (DLR-FFD)

The DLR-FFD is a virtual concept of a highly agile, manned next-generation fighter with low radar and infrared signature. The twin-engine configuration is designed to fulfill a Combat Air Patrol (CAP) mission with a radius of 550 nautical miles, relying solely on internal fuel [16]. The platform is based on parameters developed within the DLR project *Diabolo* (version V3.2.0) and was designed using the conceptual aircraft design software VAMPzeroF [17]. A visual representation of the configuration is shown in Figure 1.

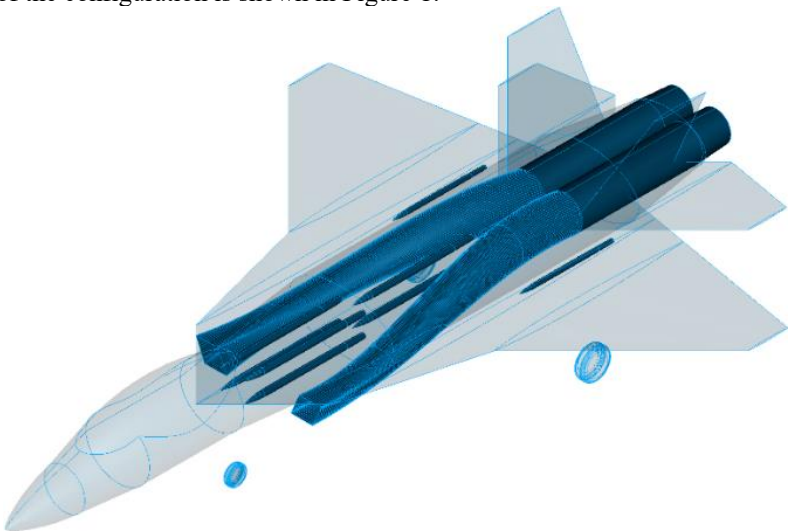

Figure 1: DLR-FFD illustration with highlighted engines and intakes

The aircraft design is tailored to the requirements of modern mission scenarios, which include extended cruise and loiter phases as well as short-duration high-power segments. In addition to the CAP mission, a Supercruise Intercept (SI) mission is considered to account for thermal peak loads. The various flight phases are approximated using a set of

DOI: 10.13009/EUCASS2025-191

simplified representative operating points (ROPs), numbered 1 through 16, allowing for efficient off-design performance evaluations of engine and TMS performance throughout the missions. The corresponding mission segments and performance parameters – thrust, Mach number, distance and altitude – are summarized in Table 1.

Table 1: Summary of the CAP and SI flight mission and representative operating points (ROPs).

Combat Air Patrol (CAP) – take-off aircraft mass 28,200 kg					
Segment	**Altitude [m]**	**Ma [–]**	**Duration [s]**	**Distance [km]**	**req. Thrust**
Take-Off **(1)**	0	0.19	26	1.5	max dry
ClimbOut **(2)**	6309	0.53	290	48.3	max dry
CruiseOut **(3)**	11000	0.85	3869	970.3	T/W = 0.43
Patrol **(4)**	10668	0.8	3600	854.0	T/W = 0.44
Acceleration **(5)**	11671	1.09	40	10.7	T/W = 2.77 (wet)
Turn1 **(6)**	11671	1.21	68	24.2	T/W = 3.23 (wet)
Turn2 **(7)**	10668	0.9	51	13.6	T/W = 2.98 (wet)
			payload drop (-154 kg)		
ClimbIn **(8)**	11482	0.9	300	79.9	T/W = 0.60
CruiseIn **(9)**	12192	0.9	3535	938.7	T/W = 0.50
Supersonic Intercept (SI) – take-off aircraft mass 26,000 kg					
Take-Off **(10)**	0	0.21	23	1.3	max dry
Acceleration **(11)**	460	0.63	17	3.0	max wet
ClimbOut **(12)**	6246	1.12	59	17.2	max wet
Supercruise **(13)**	11000	1.2	1773	628.0	T/W = 1.79
ClimbMax **(14)**	12192	1.21	24	6.4	max wet
Turn1 **(15)**	12192	1.4	47	19.0	T/W = 3.0 (wet)
			payload drop (-154 kg)		
CruiseIn **(16)**	10973	0.85	2583	648.2	T/W = 0.45

Following the approach presented in [15], it is assumed that sufficient installation space is available within the DLR-FFD to incorporate an engine-integrated TMS. A retrofit-approach is pursued, in which the two engine configurations under investigation are interchangeable within the same aircraft design. This enables a direct comparison of engine performance and thermal capability under identical aircraft constraints. It should be noted, however, that the aircraft configuration has only been optimized for the conventional engine architecture. As a result, the full system-level benefits of the VCE cannot be exploited, since the airframe has not been optimized for the more efficient propulsion architecture. Potential cascading effects – such as reduced fuel volume requirements, different take-off mass, or downsized structural components – are not captured within the current configuration. These effects could, in principle, lead to a lighter and more compact aircraft design, but remain unaccounted for in this study due to the lack of an integrated aircraft-engine optimization loop.

Moreover, the authors acknowledge that the integration of different TMS architectures may introduce cascading effects on the overall aircraft design, such as additional volume or mass penalties, which would require further airframe adaptation. Nevertheless, the focus of this study is a quantitative comparison of cooling performance between a conventional and a VCE-based engine configuration. Since the TMS cooling capability is primarily driven by the thermodynamic conditions in the bypass, no iterative aircraft redesign as described in [18] was performed.

3.2 Future Fighter Engine (DLR-FFE)

The DLR-FFE is a modern two-spool mixed-flow turbofan with an afterburner, designed for an advanced technological level through a multidisciplinary design process. An engine-aircraft coupled design process was used to iteratively define its thermodynamic cycle, enabling system-level optimization with the aim to minimize overall aircraft weight. A detailed description of the engine design methodology, boundary conditions, technological constraints, and supporting design studies can be found in [18].

The engine features a high overall pressure ratio and elevated turbine inlet temperatures, resulting in bypass temperatures of up to 500 K, posing a significant challenge for heat rejection via conventional heat exchangers. The engine simulation was performed using the modular software environment *Gas Turbine Laboratory* (GTlab) [19], developed at the DLR *Institute of Propulsion Technology* (DLR-AT). GTlab enables flexible simulations of gas turbine engines at different levels of fidelity. The design process of the engines also includes preliminary flowpath sizing and engine mass estimation [18,20].

DOI: 10.13009/EUCASS2025-191

The current DLR-FFE v4 configuration represents the result of multiple iterations between engine and aircraft design and reflects a compromise between the most demanding requirements across critical operating points [18]. The engine delivers a dry thrust of 112.7 kN (or 177.1 kN with afterburner), with a fan diameter of 1 m, and has an estimated engine mass of approximately 1.9 t. A schematic of the geometric predesign is shown in Figure 2 (top).

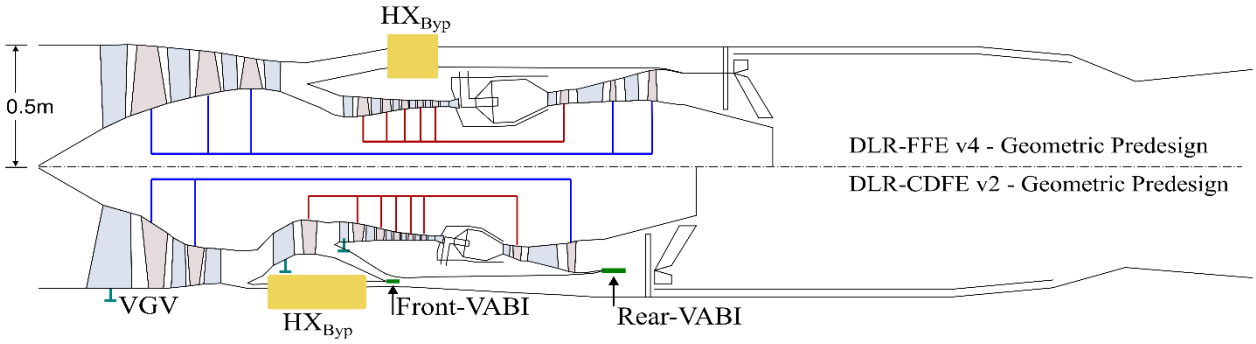

Figure 2: Geometric predesign and architectural overview of the DLR-FFE and DLR-CDFE

3.3 Core-Driven Fan Engine (DLR-CDFE)

In contrast to the conventional mixed-flow turbofan, the VCE architecture features a fan stage that is mechanically driven by the high-pressure shaft, connected to the high-pressure turbine ("core-driven fan"), while the front fan is implemented as a two-stage unit [21]. The two bypass streams, fed by the front fan and the core-driven fan, are merged using a variable-area bypass injector (VABI) before mixing with the core stream at the afterburner inlet. The basic layout of this architecture is shown in Figure 2 (bottom). The compressors (front fan, core-driven fan, and high-pressure compressor) are equipped with variable guide vanes (VGVs) to enable mass flow redistribution between the two bypass ducts. The control of this mass flow distribution makes it possible to adapt the engine operation to different operating conditions and therefore provide greater flexibility.
This configuration offers the potential for reduced bypass temperatures, even during high-power conditions, since the outer bypass stream – located downstream of the front fan – operates at a lower pressure ratio and temperature level. However, the absolute cooling capacity is limited due to the reduced mass flow in the outer bypass, which must be considered during the design and integration of heat exchangers. It should also be noted that the available radial space for a bypass heat exchanger is restricted by the underlying core-driven fan, requiring a more compact design than in the conventional FFE configuration.
The thermodynamic design of the DLR-CDFE v2 follows the retrofit approach mentioned in Section 3.1. The outer engine diameter of the conventional DLR-FFE was imposed as a constraint, and design parameters as well as variable geometries (VGVs, VABIs, nozzle) were optimized using the aircraft sensitivities presented in [18]. Compared to the DLR-FFE, the DLR-CDFE requires significantly more design and control variables – such as the bypass ratio of both bypass streams, variable VGVs, and VABIs, which necessitated an extension of the engine design methodology presented in [18]. The resulting optimization framework is part of an ongoing PhD thesis [22] and is therefore not described in this paper.
The resulting geometric predesign is shown in Figure 2 (bottom). At a comparable engine mass of approximately 1.9 t, it enables a reduction in thrust-specific fuel consumption (TSFC) of about 8 % at cruise conditions (ROP 3), while still meeting all mission thrust requirements. The efficiency gain is attributed both to improved thermodynamic performance in part-load conditions and to reduced installation drag, including spillage and boattail effects [8,22,23].

4. Thermal Management System Model

To evaluate the performance of the TMS, a closed-loop air cooling cycle, modeled as a reverse Brayton cycle, is integrated into a bypass duct of both engine architectures. The modeling, design and sizing of the TMS follows the approach presented in the previous study [15] and is briefly summarized in the following. A schematic of the system configuration is shown in Figure 3.

DOI: 10.13009/EUCASS2025-191

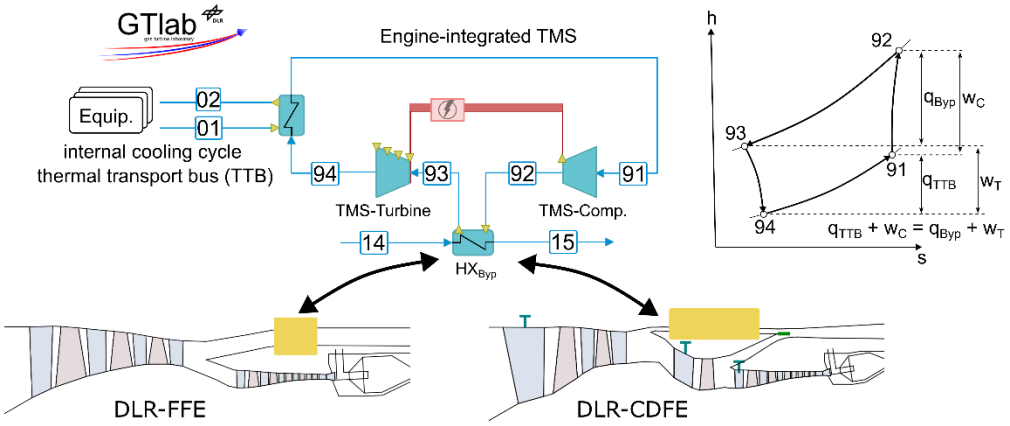

Figure 3: Thermodynamic performance model of the engine-integrated TMS and a corresponding h–s diagram

As outlined in Chapter 3, a retrofit approach is applied: the TMS architecture and airframe configuration remain fixed, while two different propulsion systems, the DLR-FFE and the DLR-CDFE, are analyzed in terms of their cooling capacity. In the case of the CDFE, the heat exchanger is installed in the outer bypass stream upstream of the bypass mixer, as illustrated in Figure 2.

The TMS uses a closed-loop cycle with an idealized cooling gas (air), which absorbs heat from the aircraft's internal thermal transport bus (TTB) via a heat exchanger (HX_{TTB}) and then discharges it into the bypass flow through a second heat exchanger (HX_{Byp}) at elevated pressure and temperature levels. Assuming adiabatic compression and expansion, the total amount of heat transferred into the bypass – referred to as the bypass heat transfer rate $\dot{Q}_{Byp}$ – can be expressed as (see also the corresponding specific quantities in the h–s diagram in Figure 3):

$$\dot{Q}_{Byp} = \dot{Q}_{TTB} + (\dot{W}_C - \dot{W}_T) \tag{1}$$

This expression highlights that the thermodynamic cycle inherently requires additional power $\dot{W}_C$ to drive the TMS-compressor. While a portion of this power is recovered by the TMS-turbine, the residual demand is covered by electrical power provided by a generator, which is driven by the high-pressure spool of the main engine. The associated power extraction reduces the available net thrust. In addition, the presence of the heat exchanger in the bypass duct causes a pressure loss as well as additional mass, further decreasing aircraft performance. A detailed quantification of these effects for the DLR-FFE has been discussed in [15].
The thermodynamic simulation of the engine-integrated TMS is performed using the modular software environment GTlab. The compressor and turbine of the TMS are modeled analogously to the main engine's turbomachinery, employing characteristic component maps. These maps are scaled at the design point and are used for off-design performance calculation and analysis.
The modeling of heat exchangers is based on the well-established P-NTU method [24]. The heat transfer rate $\dot{Q}_i$ is defined using the following relationships:

with

$$\dot{Q}_i = P_i \times C_i \times \Delta T_{max} \tag{2}$$

$$C_i = c_{p,i} \times W_i \tag{3}$$

$$\Delta T_{max} = T'_2 - T'_1 \tag{4}$$

$$P_i = \frac{\Delta T_i}{\Delta T_{max}} = \frac{|T'_i - T''_i|}{\Delta T_{max}} \tag{5}$$

In this context, T' and T'' refer to the inlet and outlet temperatures of the respective fluid, assuming $T_2 > T_1$.
The dimensionless ratio of temperature differences P_i (also referred to as effectiveness) expresses the actual temperature change of a fluid relative to the maximum possible temperature difference. This quantity is used to determine the Number of Transfer Units (NTU), which characterizes the thermal performance of a heat exchanger. The NTU represents the ratio of the heat exchanger's transfer potential to the fluid's thermal capacity rate C_i, that is, the amount of energy required to heat or cool the fluid by 1 K.

$$NTU_i = \frac{1}{1 - R_i} \cdot ln\left(\frac{1 - R_i \cdot P_i}{1 - P_i}\right) \text{ (countercurrent flow, } R \neq 1) \tag{6}$$

DOI: 10.13009/EUCASS2025-191

$$NTU_i = \frac{U \cdot A}{C_i} \tag{7}$$

$$R_i = \frac{W_i}{W_j} \tag{8}$$

The applied design and off-design methodology follow the approach that is presented in detail in [15]. The only major modification concerns the updated geometric modeling of the bypass heat exchanger. While [15] assumed a defined heat exchanger length occupying only a portion of the bypass flow, the present study considers an annular heat exchanger configuration, through which the entire bypass mass flow must pass. The estimation of the required heat exchanger volume remains identical to [15], however, because the inlet area is fixed, the axial length of the heat exchanger adapts accordingly. A reference design pressure loss coefficient $PLC_{des,ref} = 0.96$ is specified for a reference length of $L_{HX,ref} = 0.5$ m, the corresponding design pressure loss coefficient PLC_{des} is scaled linearly as follows:

$$PLC_{des}(L_{HX}) = 1 + (PLC_{des,ref} - 1) \times (L_{HX} / L_{HX,ref}) \tag{9}$$

As noted and shown in Figure 2, the DLR-CDFE architecture provides less radial installation space; hence, the radial channel height is set to $h_{HX,CDFE} = 0.1$ m, compared to $h_{HX,FFE} = 0.14$ m. As a result, for two heat exchangers with identical exchange area A_{HX}, the fluids in the CDFE configuration experience a slightly higher pressure loss due to the increased length. Sensitivity analyses showed that variations in heat exchanger size had a negligible effect on the thermodynamic cycle parameters and overall cooling capacity. Furthermore, prior results [15] showed that pressure losses in the bypass duct have a minimal impact on engine performance and are therefore not discussed further.
The simulation setup described here forms the basis for the comparative evaluation of both engine architectures, as discussed in the following chapter.

5. Results and discussion

The cooling potential of an engine-integrated thermal-management system (TMS) is assessed for the two reference architectures DLR-FFE and DLR-CDFE. The thermodynamic design builds upon the TMS presented in [15], which was sized to deliver 25 kW at the condition with the coldest temperature in the bypass (ROP 4). For the present work the design procedure was modified:

- Design point: A representative operating point with a bypass temperature of $T_{14} = 360$ K and a required temperature reduction (cooling) of $\Delta T_{TTB} = 65$ K at a TTB inlet temperature $T_{01} = 313.15$ K (40°C) is selected.
- The design mass flow rates of the TMS and TTB are increased compared to [15], while the capacity rates C_i remain approximately equal inside the HX_{TTB}.
- The derived design (see data in Figure 4) yields a theoretical cooling capacity of $\dot{Q}_{TTB,max} = 42.6$ kW at the design point. The deliberate oversizing follows the findings in [15]: a TMS sized for the coldest mission requirement (ROP 4) may fail to provide any cooling in hot-bypass segments. The current design therefore provides higher flexibility in high-load operating points. However, an operational required cooling capacity of $\dot{Q}_{TTB} = 25$ kW is targeted in all mission points.

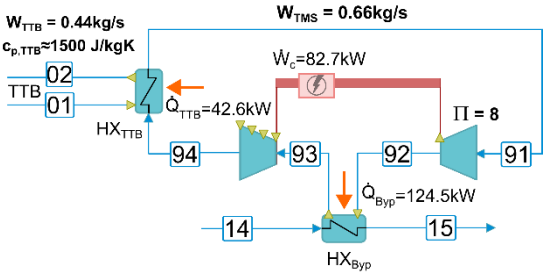

Station	Temp. [K]	pressure (atm)
01	**313**	**2.0**
02	**248**	1.96
91	296	**1.0**
92	564	8.0
93	381	7.68
94	232	1.04
14	**360**	0.86
15	368	0.82

Figure 4: Schematic of the engine-integrated TMS design including design inputs (bold) and resulting values

DOI: 10.13009/EUCASS2025-191

5.1 Cooling capacity of the DLR-FFE

Figure 5 summarizes the cooling capacity for all representative operating points across the mission as defined in Table 1. The blue bars represent the cooling capacity that the TMS could provide in the TTB heat exchanger, assuming a constant compressor power of 82.7 kW. In cases where the cooling potential exceeds the nominal requirement of 25 kW, the compressor power is reduced to adjust the cooling capacity to the target value. The resulting regulated capacities are shown in orange. This form of modulation is particularly relevant for operating points characterized by low bypass temperatures or high heat sink capacity, where overcooling would otherwise occur.

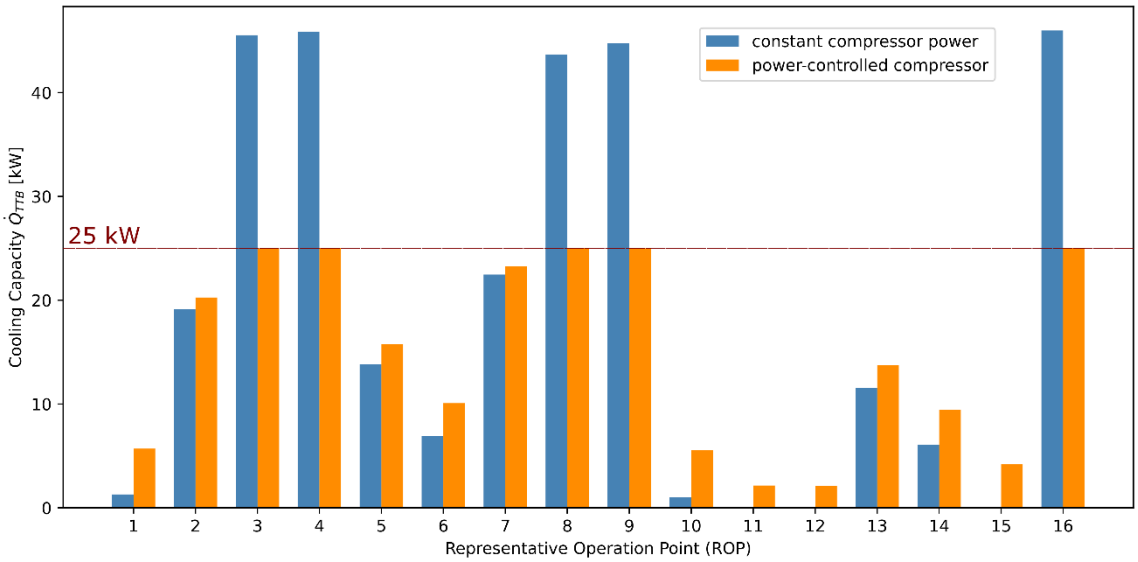

Figure 5: Cooling capacity of the DLR-FFE for all ROPs, comparing constant TMS-compressor power and power-control scheme by throttling the TMS-compressor

Interestingly, in demanding operating points with elevated bypass temperatures, where the cooling potential is lower, a reduction in compressor power can lead to an increase in effective cooling capacity. In the Supercruise segment (ROP 13), lowering TMS power from 82.7 kW to 59.1 kW increases the cooling from 11.5 kW to 13.8 kW, representing a 19 % gain. In contrast, colder segments such as Patrol (ROP 4) exhibit a monotonic decrease as the TMS-compressor power is reduced. The underlying trends are summarized in Figure 6.

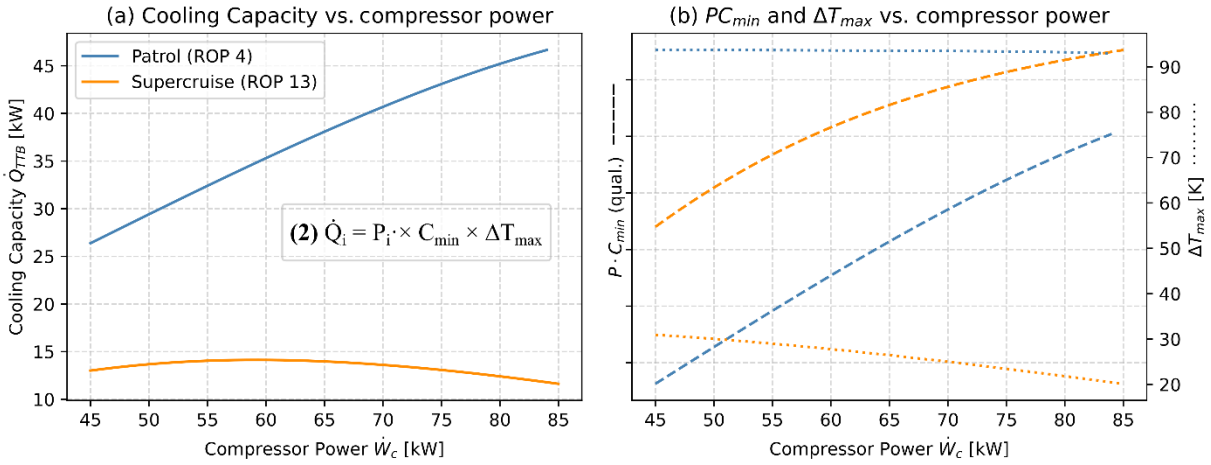

Figure 6: Change of cooling capacity **(a)**, $P \times C_{min}$ and ΔT_{max} **(b)** for a variation of TMS compressor power

DOI: 10.13009/EUCASS2025-191

As compressor power is reduced, the TMS mass flow rate decreases, which raises the NTU and thus the effectiveness P of the TTB heat exchanger. Although the capacity rate C_{min} in the heat exchanger is reduced accordingly, the product $P \times C_{min}$ continues to rise over a finite range. At the same time, the turbine outlet temperature T_{94} is lower in supercruise, because the TMS-compressor pressure ratio drops while the TMS-turbine still operates close to its peak efficiency at the lower flow rate. The resulting increase in temperature difference $\Delta T_{max} = T_{01} - T_{94}$ further enhances the cooling potential, so that the term $P \times C_{min} \times \Delta T_{max}$ (Eq. 2) reaches a maximum at moderate power settings. Beyond this point the decreasing mass flow dominates and the cooling capacity declines. However, in the Patrol segment (ROP 4), the lower TMS mass flow is accompanied by a decline in turbine efficiency, so that, despite a lower turbine-inlet temperature T_{93}, the turbine outlet temperature T_{94} (and hence ΔT_{max}) remains approximately unchanged.
Since this peak arises from the coupled off-design behavior of the TMS turbomachinery, it is difficult to predict based on simple proportional reasoning. This underscores the importance of selecting a feasible design point that positions the compressor and turbine in favorable regions of their characteristic maps, and highlights the need for accurate component design and sizing in the conceptual design phase of engine-integrated TMS.

5.2 Cooling capacity of the DLR-CDFE and comparison

Figure 7 presents the resulting cooling capacity of the DLR-CDFE for all representative operating points (ROPs). As in Figure 5, blue bars correspond to a constant TMS-compressor power, while orange bars include the compressor power-control strategy introduced in Section 5.1. The underlying variability schedule (VGVs and VABIs) was optimized for minimum mission fuel burn.

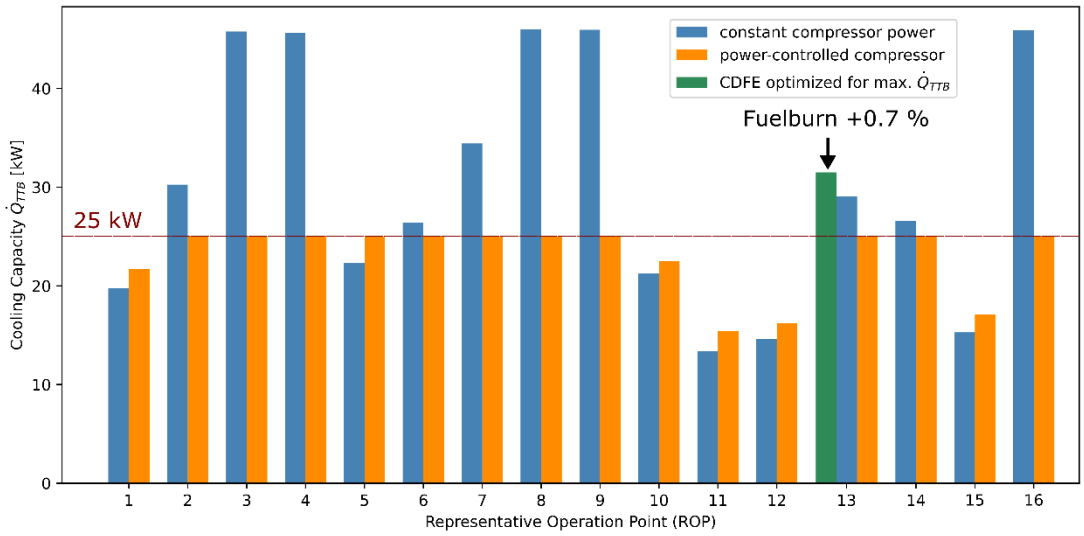

Figure 7: Cooling capacity of the DLR-CDFE for all ROPs, comparing constant TMS-compressor power and power-control scheme by throttling the TMS-compressor

With this schedule the DLR-CDFE meets the 25 kW requirement in eleven of the sixteen ROPs. The five points that do not meet the requirement occur exclusively in the hottest, low-altitude segments (ROPs 11, 12, 15 and two take-off points 1 and 10). Even in those cases, however, the shortfall is significantly reduced compared to the FFE. Under supercruise conditions (ROP 13) the gain is particularly striking: the CDFE delivers the full 25 kW, whereas the FFE architecture only reaches 13.8 kW under identical constraints. The improvement stems from different bypass conditions. Within the CDFE, the bypass temperature drops from T_{14} = 458 K (FFE) to 406 K, while the bypass mass flow decreases from W_{14} = 28.8 kg/s (FFE) to 6.3 kg/s. Generally, a trade-off can be expected in this context: while a colder heat sink improves cooling effectiveness, excessively low mass flow rates can limit the amount of heat that can be transferred into the bypass. To visualize this trade-off, Figure 8 shows the bypass heat transfer rate ($\dot{Q}_{Byp}$) for a fixed TMS state (NTU = 1.83, W_{TMS} = 0.84 kg/s, T_{93} = 575 K) as a function of T_{14} and W_{14} according to Eq. (2-5). The plot demonstrates that, once the bypass flow rate greatly exceeds the TMS flow rate ($W_{14} \gg W_{TMS}$), further gains in cooling are governed almost exclusively by lowering the bypass temperature. Furthermore, a cooler bypass directly increases the heat removal potential in the HX_{TTB}, thereby increasing the cooling capacity $\dot{Q}_{TTB}$.

DOI: 10.13009/EUCASS2025-191

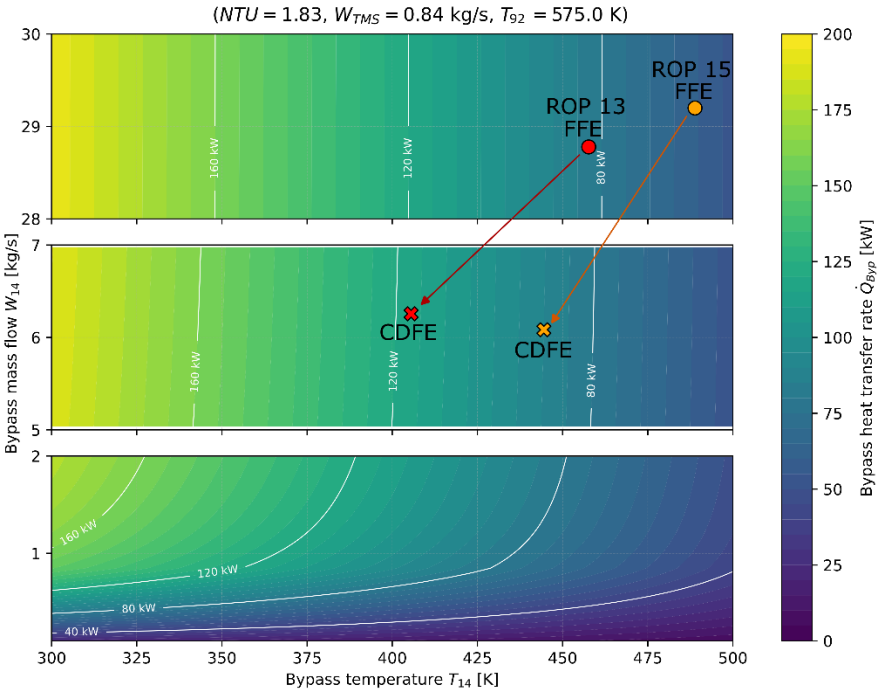

Figure 8: Change of the bypass heat transfer rate as a function of bypass mass flow and temperature for fixed TMS conditions, red and orange markers indicate the change of bypass conditions between DLR-FFE and DLR-CDFE

While this estimation of the bypass heat transfer rate is based on fixed TMS boundary conditions; in reality parameters such as NTU, W_{TMS} and T_{92} vary for different operating points. Nevertheless, the chosen reference values give a robust first-order estimate of the cooling potential that is independent of the detailed TMS design and can already be employed during the initial sizing and optimization phase of the CDFE variability schedule.
To illustrate the flexibility of VCE, the variability schedule was re-optimized with the sole objective of maximizing $\dot{Q}_{Byp}$ according to Eq. (2-5) under identical technological constraints. For Supercruise (ROP 13) the resulting schedule lowers the bypass temperature further to 398 K; the predicted maximum cooling rises to $\dot{Q}_{TTB}$ = 31.5 kW, i.e. +7.7 % relative to the fuel burn optimized schedule (29.1 kW). The higher potential is shown as the green bar in Figure 7. Mission fuel burn increases by only 0.7 %, demonstrating that optimization of variabilities can unlock substantial thermal management benefits at minimal performance penalties.

6. Conclusion

This paper examined an engine-integrated thermal management system (TMS), modeled as a closed reverse Brayton cycle, in combination with two different fighter engine architectures. Building on prior work [15], which analyzed the trade-offs between engine performance, TMS design parameters and cooling capacity in detail, the present study focused specifically on comparing the achievable cooling potential. In particular, the influence of different bypass boundary conditions on cooling performance was investigated by comparing a conventional mixed-flow turbofan with a variable-cycle engine (VCE) architecture. Sixteen representative operating points were derived from two flight missions, using a uniform 25 kW cooling demand as a reference for system comparison.
For the VCE, whose variability schedule was optimized for minimum fuel burn at each operating point, significantly higher cooling capacities were observed. Under supercruise conditions, for instance, the VCE delivered twice the cooling capacity of the conventional reference engine, thereby meeting the full 25 kW requirement. Only in the most demanding hot- and low-altitude segments did the TMS fail to meet the target, yet it consistently outperformed the conventional reference.
The improvement was explained using a simplified estimation of the possible bypass heat transfer rate. The results showed that when the bypass mass flow significantly exceeds the TMS flow ($W_{Byp} \gg W_{TMS}$), the cooling capacity is primarily governed by the bypass temperature: lower temperatures (heat sinks) yield greater heat rejection rates.
Using the P-NTU method under fixed NTU and mass flow conditions enabled a computationally efficient estimation of the bypass heat transfer rate, which supported the optimization of the VCE variability schedule. Re-optimization for maximum bypass heat transfer rate under identical boundary constraints led to an additional 7.7 % increase in cooling capacity at supercruise, with a fuel-burn penalty of just 0.7 %. This result highlights the flexibility of VCEs to adapt to varying flight conditions and mission objectives through control of variable devices.

DOI: 10.13009/EUCASS2025-191

Furthermore, it was found that the design and control of turbomachinery within the TMS can strongly affect off-design performance. In particular, throttling the TMS compressor led to increased cooling capacity in several cases. This underscores the importance of carefully selecting component designs and understanding their off-design characteristics. Future studies will include refined turbomachinery and heat exchanger models, as well as improved estimation of component mass and installation space. As part of the WingMates project, these developments will support the integrated design of a holistic power and thermal management system for a virtual next-generation fighter configuration.

References

[1] Jafari, S. and Nikolaidis, T. Thermal Management Systems for Civil Aircraft Engines: Review, Challenges and Exploring the Future. Appl. Sci. 8(11)2044, 2018.

[2] Dooley M., Lui, N., Newman, R., and Lui, C., Aircraft Thermal Management -Heat Sink Challenge SAE Technical Paper 2014-01-2193, 2014.

[3] van Heerden, A.S.J., Judt, D.M., Jafari, S., Lawson C.P., Nikolaidis T. and Bosak, D. Aircraft thermal management: Practices, technology, system architectures, future challenges, and opportunities. In: *Progress in Aerospace Sciences, Vol. 128*, 2022.

[4] Iden, S., Sehmbey, M., and Borger, D., MW Class Power System Integration in Aircraft. SAE Technical Paper 2004-01-3202, 2004.

[5] Warwick, G. New AFRL Program Focuses on Aircraft Energy Issues. In: *Aviation Week &Space Technology, vol. 172, no. 25*, 2010.

[6] Clark, R. A Method for the Conceptual Design of Integrated Variable Cycle Engines and Aircraft Thermal Management Systems. Ph.D. dissertation, Georgia Institute of Technology, 2023.

[7] Clark, R. A., Tai, J., and Mavris, D. Integrated Design of a Variable Cycle Engine and Aircraft Thermal Management System. In: *ASME. J. Eng. Gas Turbines Power*, 2024.

[8] Zenkner, S., Carvalho, F., Brakmann, R. G., and Goinis, G. Variable Cycle Engine Concepts and Component Technologies—An Overview. In: *ASME. J. Eng. Gas Turbines Power 147(5): 051004*. 2024.

[9] Ganev, E. and Koerner, M. Power and Thermal Management for Future Aircraft. SAE 13ATC-0280, 2013.

[10] Bisht, I. S. Honeywell Demonstrates Upgrading F-35's Cooling System, online available: https://thedefensepost.com/2024/03/15/honeywell-f35-cooling-system/, 2024.

[11] Marrow, M. Honeywell unveils new F-35 thermal management fix as Pentagon hunts for better cooling, online available:https://breakingdefense.com/2024/03/honeywell-unveils-new-f-35-thermal-management-fix-as-pentagon-hunts-for-better-cooling/, 2024.

[12] Marrow, M. Lockheed eyes two-year timeline to pick new F-35 cooling system, online available: https://breakingdefense.com/2025/03/lockheed-eyes-two-year-timeline-to-pick-new-f-35-cooling-system/, 2025.

[13] Marrow, M. It's official: The F-35 will not get a new engine anytime soon, online available: https://breakingdefense.com/2024/03/its-official-the-f-35-will-not-get-a-new-engine-anytime-soon/, 2024.

[14] Corbett, M. Shaft Power Extraction and Waste Heat Rejection using a Three Stream Variable Cycle Engine, In: *SAE Int. J. Aerosp. 5(2):371-385*, 2012.

[15] Matuschek, T.; Häßy, J.; Schmelcher, M.; Görtz, A., Performance Assessment of an Engine-Integrated Closed-Air Cooling Thermal Management System in a Next Generation Fighter Configuration, In: *34th Congress of the International Council of the Aeronautical Sciences, ICAS* 2024.

[16] Liersch, C. M., Schütte, A., Moerland, E., and Kalanja, M. DLR Project Diabolo: An Approach for the Design and Technology Assessment for Future Fighter Configurations. In: *AIAA AVIATION 2023 Forum*, p. 3515, 2023.

[17] Mancini, A., Zamboni, J. and Moerland, E. A knowledge-based methodology for the initiation of military aircraft configurations. In: *American Institute of Aeronautics and Astronautics (AIAA) AVIATION Forum*, 2021.

[18] Matuschek, T., Otten, T., Zenkner, S., Becker, R., Zamboni, J., and Moerland, E. Application of a Multidisciplinary Design Process to Assess the Influence of Requirements and Constraints on the Design of Military Engines. In: *ASME. J. Eng. Gas Turbines Power*. 2024.

[19] Reitenbach, S., Becker, R., Hollmann, C., Wolters, F., Vieweg, M., Schmeink, J., Otten, T., and Siggel, M. Collaborative Aircraft Engine Preliminary Design using a Virtual Engine Platform, Part A: Architecture and Methodology. In: *AIAA SciTech Forum*, 2020.

[20] Häßy, J., Schmeink, J. Knowledge-Based Conceptual Design Methods for Geometry and Mass Estimation of Rubber Aero Engines. *33rd Congress of the International Council of the Aeronautical Sciences (ICAS)*, Stockholm, Sweden, 2022.

[21] Johnson, J. Variable Cycle Engine Concepts. *AGARD PEP Symposium on "Advanced Aero-Engine Concepts and Controls"*. 1995.

[22] Zenkner, S. Preliminary design, optimization and comparison of variable cycle engines for a supersonic aircraft, Doctoral dissertation in preparation, Universität der Bundeswehr München (UniBwM), expected 2026.

DOI: 10.13009/EUCASS2025-191

[23] Hönes, S. Analyse des Potenzials von VCE-Triebwerken zur Reduktion der Installationswiderstände von Triebwerkseinlauf und -düse. master thesis, Universität Stuttgart, 2022.
[24] Stephan, P., Kabelac, S., Kind, M., Mewes, D., Schaber, K. and Wetzel, T. VDI-Wärmeatlas mit 1046 Abbildungen und 483 Tabellen. 12. Auflage, Springer Vieweg, p.39-97, 2019.